Preprints.org | NOT PEER-REVIEWED | Posted: 19 November 2026 https://doi.org/10.20944/preprints202611.1989.v1

Disclaimer/Publisher's Note: The statements, opinions, and data contained in all publications are solely those of the individual author(s) and contributor(s) and not of MDPI and/or the editor(s). MDPI and/or the editor(s) disclaim responsibility for any injury to people or property resulting from any ideas, methods, instructions, or products referred to in the content.

Article

Real-Time Registration of Horseradish Peroxidase Activity Using a Solid-State Nanopore-Based Electrical Detector

Ekaterina T. Efimova [1], Ivan D. Shumov [1,*], Vadim S. Ziborov [1,2], Alexander Y. Dolgoborodov [2], Oleg F. Petrov [2], Alexander N. Ableev [1], Andrey F. Kozlov [1], Amilia A. Samitova [1], Ekaterina E. Vazhenkova [1], Maria A. Agletdinova [1], Irina T. Utkina [1], Oleg N. Afonin [1], Nikita V. Vaulin [3], Denis V. Lebedev [3], Anton S. Bukatin [3], Ivan S. Mukhin [3], Vadim Y. Tatur [4], Andrei A. Lukyanitsa [4,5], Nina D. Ivanova [6], Anna V. Grudo [7], Alexander I. Archakov [1] and Yuri D. Ivanov [1,2,*]

[1] Institute of Biomedical Chemistry, 10, Pogodinskaya st., Moscow, 119121 Russia
[2] Joint Institute for High Temperatures of the Russian Academy of Sciences, 13 Bd.2, Izhorskaya st., Moscow, 125412 Russia
[3] Laboratory of Renewable Energy Sources, St. Petersburg Academic University, 8/3, Khlopina St., 194021 St. Petersburg, Russia
[4] Foundation of Perspective Technologies and Novations (FPTN), 8 bld. 1, 2nd Ambulatorny rd., Moscow, 125315 Russia
[5] Faculty of Computational Mathematics and Cybernetics, Lomonosov Moscow State University, Leninskie Gory, 1, Moscow, 119991, Russia
[6] Moscow State Academy of Veterinary Medicine and Biotechnology Named after Skryabin, 23, Academician Skryabin st., Moscow, 109472 Russia
[7] Institute of Bioorganic Chemistry, National Academy of Sciences of Belarus, 220084 Minsk, Belarus
* Correspondence: shum230988@yandex.ru (I.D.S); yurii.ivanov.nata@gmail.com (Y.D.I.).

Abstract

Real-time tracking of enzymatic activity of horseradish peroxidase (HRP) in the reaction of 2,2′-azino-bis(3-ethylbenzothiazoline-6-sulfonate) (ABTS) oxidation by hydrogen peroxide was been performed in 0.1 M KCl using a (solid state nanopore)-based sensor device (SSNPSD). The SSNPSD comprised a silicon nitride (Si_3N_4) chip with a solid-state nanopore. The enzyme has been introduced into the cis-chamber of the sensor's measuring cell under a positive voltage relative to the trans-chamber. The adsorption of HRP onto mica from 0.1 M KCl has been studied by atomic force microscopy (AFM). In parallel, the enzymatic activity of HRP under experimental conditions has been confirmed by spectrophotometry. In addition, the spectrophotometry-based technique has been employed in order to check the enzyme's functionality at various values of pH and ionic strength. Our experiments reported herein demonstrate the applicability of Si_3N_4 chip-based SSNPSD for monitoring the activity of single enzyme molecules by measuring fluctuations in the electric current passing through the nanopore during the enzyme functioning. By spectrophotometry, the functionality of the enzyme in chloride-containing buffer solutions with acidic and basic pH has been confirmed in order to determine the possibility of nanopore-based activity studies at these pH values. In AFM and spectrophotometry experiments, cytochrome P450 CYP102A1 (P450 BM3) has been employed as a reference enzyme. The results reported represent an important step towards single-molecule studies of enzymatic processes.

Keywords: horseradish peroxidase; solid state nanopore; enzymatic activity; spectrophotometry; single-molecule enzymology

© 2026 by the author(s). Distributed under a Creative Commons CC BY license.

Preprints.org | NOT PEER-REVIEWED | Posted: 19 November 2026 https://doi.org/10.20944/preprints202611.1989.v1

1. Introduction

Single-molecule studies of enzymes are of importance for understanding mechanisms of enzymatic catalysis [1–3]. These studies can be performed by atomic force microscopy (AFM) [4,5] and by using nanopore-based detectors [6–9], including those based on solid-state nanopores [2,3,10–12]. While the AFM-based single-molecule studies of enzymes are considerably laborious, implementation of nanopore-based experiments is much simpler. The application of natural nanopores, which are formed in lipid bilayer membranes with use of pore-forming proteins such as outer membrane protein G [6] or alpha-hemolysin [7–9]. The major drawback of such natural nanopores is their limited size determined by the structure of pore-forming protein; the pore size constraints limit the list of enzymes, which can be studied with the natural nanopores. The second drawback of the natural nanopores is their limited time stability [12]. In contrast, the use of solid-state nanopores formed in inorganic chips allows the researchers to overcome the limitations typical for the natural nanopores [2–4,10–13].

In our study reported herein, a detector based on solid-state nanopore formed in silicon nitride (Si_3N_4) chip has been employed for real-time monitoring of enzymatic activity of horseradish peroxidase in the reaction of 2,2′-azino-bis(3-ethylbenzothiazoline-6-sulfonate) (ABTS) oxidation by hydrogen peroxide. This enzyme has found numerous applications in biotechnology and biomedicine [14,15], and peroxidases in general play an important role in food technology [14]. This motivates extensive studies of its catalytic properties.

2. Materials and Methods

2.1. Reagents

Potassium chloride (KCl) was from Fluka (Germany). Potassium tetraborate was from Acros Organics (Geel, Belgium). Hydrogen peroxide (H_2O_2), potassium dihydrophosphate (KH_2PO_4), potassium hydroxide (KOH), citric acid and acetic acid were from Reakhim (Russia). The HRP enzyme (Cat. # P6782) and its substrate 2,2′-azino-bis(3-ethylbenzothiazoline-6-sulfonate) (ABTS), and sodium laurate were from Sigma (USA). The CYP102A1 enzyme was also expressed by Dr. A.V. Grudo [4]. Dulbecco's modified phosphate buffered saline (PBSD) was prepared using a salt premix commercially available from Pierce (USA). All chemicals were of analytical or higher purity grade unless otherwise specified. All solutions were prepared with ultrapure deionized water obtained with a Simplicity UV system (Millipore, Molsheim, France). The pH of all solutions was checked with an Ekspert-001 liquid analyzer (Ekonix-Expert, Moscow, Russia) equipped with a combined pH-sensitive glass electrode (Izmeritelnaya Tekhnika, Moscow, Russia). Muscovite mica was purchased from SPI (USA) in the form of standard 75 × 25 mm slides, which were cut into 7 × 15 mm pieces. Highly oriented pyrolytic graphite (HOPG; ZYH grade) was from Tips Nano (Estonia).

2.2. Measurements with the Nanopore Sensor

The (solid state nanopore)-based sensor device (SSNPSD) comprised a poly(tetrafluoroethylene) measuring cell divided into two 250 μL chambers (the cis-chamber and the trans-chamber) by a 40-m-thick Si_3N_4 chip with a solid-state nanopore. The 5-nm-wide nanopore was formed in the chip with a JEM 2100F transmission electron microscope (JEOL, Japan). The nanopore diameter was subsequently increased to 9 or 16 nm by etching of the chip with piranha solution. The cis- and trans-chambers of the cell were filled with a 0.1 M KCl solution. Ag/AgCl electrodes were immersed into the solution in the chambers in order to perform measurements of the ionic current flowing through the nanopore. The ionic current was measured with either a home-made patch-clamp amplifier with an intrinsic noise level of 0.3 pA (at a 1 kHz bandwidth) or with an Axopatch 200B patch-clamp amplifier (Axon Instruments, USA) operated at a 5 kHz bandwidth. The signal from the pore was recorded at a sampling rate of 10 kHz using a 16-bit ADC. Subsequently, the signal was digitally

© 2026 by the author(s). Distributed under a Creative Commons CC BY license.

Preprints.org | NOT PEER-REVIEWED | Posted: 19 November 2026 https://doi.org/10.20944/preprints202611.1989.v1

filtered using a low-pass Butterworth filter with a cutoff frequency of 1000 Hz. The layout of the SSNPSD setup is described in detail elsewhere [16].

Prior to the experiments, the both chambers of the measuring cell were filled with 250 μL of pure 0.1 M KCl solution. In the experiments with the enzyme, HRP was added to the solution in the cis-chamber to reach the final enzyme concentration of 1 μM. The solutions of ABTS and H_2O_2 were subsequently added to concentrations of 0.3 mM and 2.5 mM, respectively. Blank experiments were performed in the absence of the enzyme in the cis-chamber.

2.3. Atomic Force Microscopy

Direct surface adsorption [17] of HRP onto mica from 0.1 M KCl buffer was studied by AFM with an NT-MDT NTEGRA Prima atomic force microscope (NT-MDT, Zelenograd, Russia) equipped with gold-coated NSG-10 cantilevers (Tips Nano, Estonia). AFM scanning was performed in tapping mode in air. The direct surface adsorption experiments were performed exactly as described previously [18], but 0.1 M KCl solution was used instead of 2 mM PBSD. In the case with CYP102A1, the enzyme was adsorbed onto HOPG from 0.5 μM solution in either 2 mM PBSD or 0.1 M KCl.

Distribution $\rho(h)$ of mica-adsorbed enzyme particles with height were calculated as described in our previous papers [3,18].

2.4. Spectrophotometry

Spectrophotometric measurements were performed with an Agilent 8453 spectrophotometer (Agilent Deutschland GmbH, Waldbronn, Germany) in 1-cm-long quartz cell.

The reactions of HRP-catalyzed oxidation of ABTS by H_2O_2, and of CYP102A1-catalyzed monooxygenation of laurate in the presence of NADPH, were performed in either of the following media: ultrapure water; 0.06 M, 0.14 M or 0.6 M KCl (pH 5.5); 2 mM or 10 mM PBSD; 1 mM potassium acetate buffer (pH 4.0); 1 mM potassium borate buffer (pH 8.2).

In the case with HRP, ABTS was preliminary dissolved in each of the solutions used in the measurements; a 30 μL volume of 0.1 μM HRP solution in 0.1 M KCl was added to the solution in the cell and thoroughly stirred. The reaction was initiated by adding 8.5 μL of H_2O_2 to its final concentration in the cell of 2.5 mM. The spectrum acquisition was started immediately after H_2O_2 addition [18].

In the case of CYP201A1, sodium laurate was preliminary dissolved in each of the solutions used in the measurements; a 1.5 μL volume of initial 80 μM CYP102A1 solution was then pipetted into the cell and thoroughly stirred. The reaction was initiated by adding 30 μL volume of 14.9 mg/mL NADPH solution. The final concentrations of CYP102A1, sodium laurate and NADPH in the cell were 40 nM, 500 μM, and 200 μM, respectively. The decrease in absorbance at 340 nm was then monitored [4].

3. Results and Discussion

3.1. AFM Study of Enzyme Adsorption

Figure 1 displays typical AFM image, and $\rho(h)$ distribution of HRP particles adsorbed on mica from 0.1 M KCl.

© 2026 by the author(s). Distributed under a Creative Commons CC BY license.

Preprints.org | NOT PEER-REVIEWED | Posted: 19 November 2026 https://doi.org/10.20944/preprints202611.1989.v1

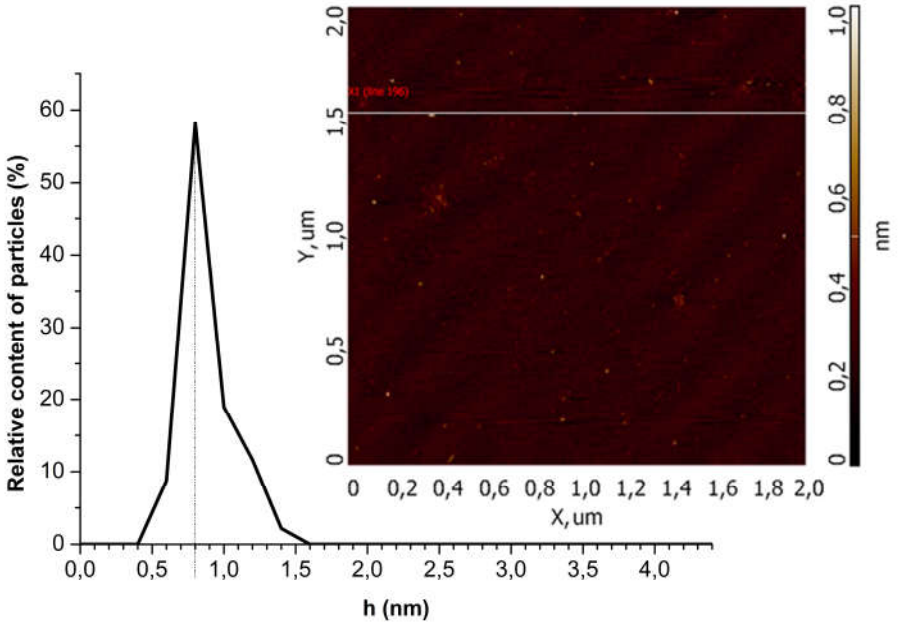

Figure 1. Distribution $\rho(h)$ and typical AFM image of HRP particles adsorbed on mica from 0.1 M KCl.

The AFM data shown in Figure 1 indicate that from 0.1 M KCl, the enzyme adsorbs on mica predominantly in monomeric form, since the $\rho(h)$ distribution of mica-adsorbed HRP has a single maximum at h = 0.8 nm.

In contrast to HRP, in our experiments reported, CYP102A1, in its turn, did not adsorb on mica at all; its adsorption was only observed on HOPG. This phenomenon allows us to suppose that in our experiments, the adsorption of CYP102A1 is governed by hydrophobic interactions. Figure 2 displays typical AFM images, and $\rho(h)$ distributions of CYP102A1 particles adsorbed on HOPG from 0.1 M KCl and 2 mM PBSD.

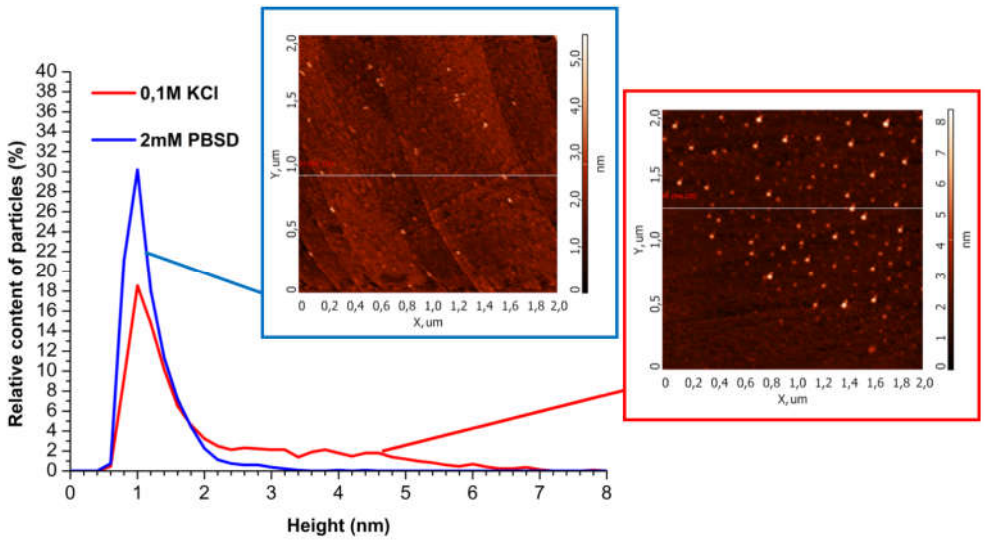

Figure 2. Distribution $\rho(h)$ and typical AFM image (right) of HRP particles adsorbed on mica from 0.1 M KCl.

The data presented in Figure 2 indicate that 2 mM PBSD, CYP102A1 adsorbs predominantly in its monomeric form with maximum of the $\rho(h)$ distribution corresponding to h_{max} = 1.0 nm. In contrast, from 0.1 M KCl, CYP102A1 adsorbs as a mixture of monomeric form of the enzyme with its aggregated forms with heights of up to 6.8 nm.

© 2026 by the author(s). Distributed under a Creative Commons CC BY license.

Preprints.org | NOT PEER-REVIEWED | Posted: 19 November 2026 https://doi.org/10.20944/preprints202611.1989.v1

3.2. Passage of Monomeric HRP Through 16-nm-wide Nanopores

Firstly, experiments with larger (16 nm) nanopores have been performed. In these experiments, the home-made patch-clamp amplifier characterized by a 1 kHz bandwidth was employed. Figure 3 displays typical time dependence of ionic current (*I(t)* curve) recorded in the course of HRP-catalyzed oxidation of ABTS by hydrogen peroxide upon application of 200 mV potential to the solution in the cis-chamber of the measuring cell. All components of the enzymatic reaction were added to the 0.1 M KCl solution in the cis-chamber.

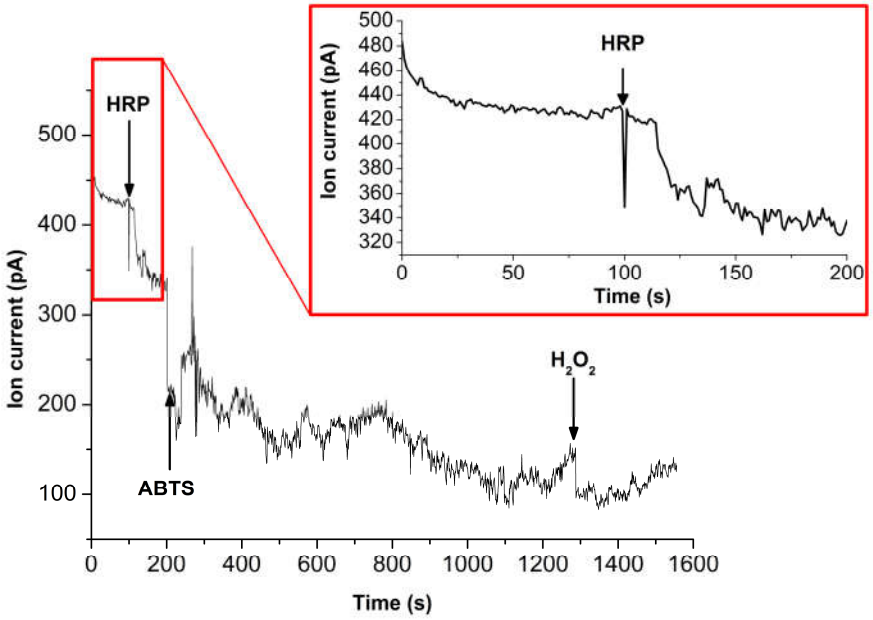

Figure 3. Typical time dependence of the ionic current recorded in the course of HRP-catalyzed oxidation of ABTS by hydrogen peroxide with a home-made patch-clamp amplifier (1 kHz bandwidth) using a Si_3N_4 chip with a 16-nm-wide nanopore. Arrows indicate time points of addition of the enzymatic reaction components to the solution in the cis-chamber of the measuring cell. Experimental conditions: 200 mV potential was applied to the cis-chamber; reaction medium was 0.1 M KCl solution (pH 5.5). The final concentrations of the HRP, ABTS and H_2O_2 in the cis-chamber were 1 μM, 0.3 mM and 2.5 mM, respectively. Inset shows the enlarged fragment of the *I(t)* curve marked with the red box.

The *I(t)* curve shown in Figure 3 indicates a considerable decrease in the ionic current accompanied with an increase in the amplitude of ionic current fluctuations after the addition of HRP into the cis-chamber to the concentration of 1 mM. Importantly, subsequent addition of ABTS did not cause any considerable change in the curve's shape — neither did the addition of H_2O_2. This is in contrast to the situation observed with narrow (5 nm) nanopores [16].

The behaviour of the ionic current in the experiment with 16-nm-wide nanopore can be explained as follows. Addition of the enzyme caused partial shrinkage of the nanopore due to adsorption of the enzyme on its walls. Nevertheless, the nanopore's lumen remained wide enough and allowed the small (0.8-nm-high if adsorbed) enzyme monomers to pass through. And this explains the increase in the amplitude of the ionic current fluctuations: namely, the high-amplitude ionic current pulses observed after the enzyme addition can well be ascribed to passage of individual enzyme globules through the nanopore. The presence of surface-adsorbed enzyme on the pore walls also explains that ionic current fluctuations were observed even after switching the potential applied to the cis-chamber to –200 mV (Figure 4). These surface-adsorbed enzyme globules continued functioning in the nanopore even at the negative potential applied. The explanation given above is also supported by the results reported by Tan et al.: namely, in 0.1 M KCl, HRP exists in monomeric form, and thus single enzyme particles pass through 28-nm-wide nanopores formed in Si_3N_4 [13].

© 2026 by the author(s). Distributed under a Creative Commons CC BY license.

Preprints.org | NOT PEER-REVIEWED | Posted: 19 November 2026 https://doi.org/10.20944/preprints202611.1989.v1

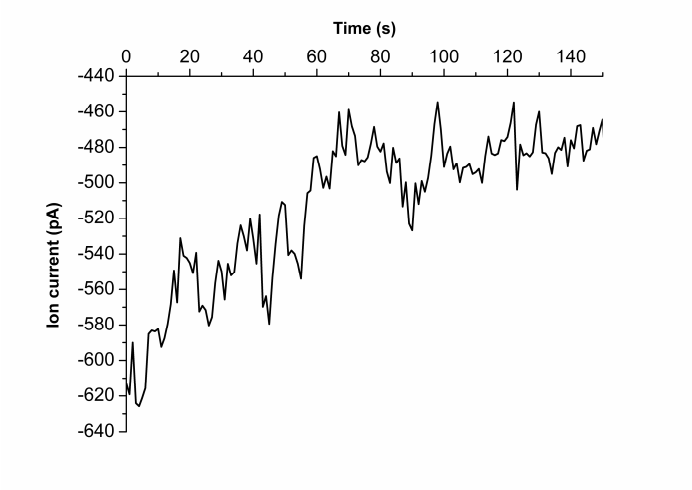

Figure 4. Typical time dependence of the ionic current recorded in the course of HRP-catalyzed oxidation of ABTS by hydrogen peroxide with a home-made patch-clamp amplifier (1 kHz bandwidth) using a Si_3N_4 chip with a 16-nm-wide nanopore. Experimental conditions: –200 mV potential was applied to the cis-chamber; reaction medium was 0.1 M KCl solution (pH 5.5). The concentrations of the HRP, ABTS and H_2O_2 in the cis-chamber were 1 μM, 0.3 mM and 2.5 mM, respectively.

3.3. Observation of HRP functioning with 9-nm-wide nanopores

Secondly, experiments with narrower (9 nm) nanopores were conducted. In these experiments, an Axopatch 200B patch-clamp amplifier (Axon Instruments, USA) operated at a 5 kHz bandwidth was employed, allowing us to record the *I(t)* curves in more detail. Figure 5 displays typical time dependence of ionic current (*I(t)* curve) recorded in the course of HRP-catalyzed oxidation of ABTS by hydrogen peroxide upon application of 400 mV potential to the solution in the cis-chamber of the measuring cell. All components of the enzymatic reaction were added to the 0.1 M KCl solution in the cis-chamber.

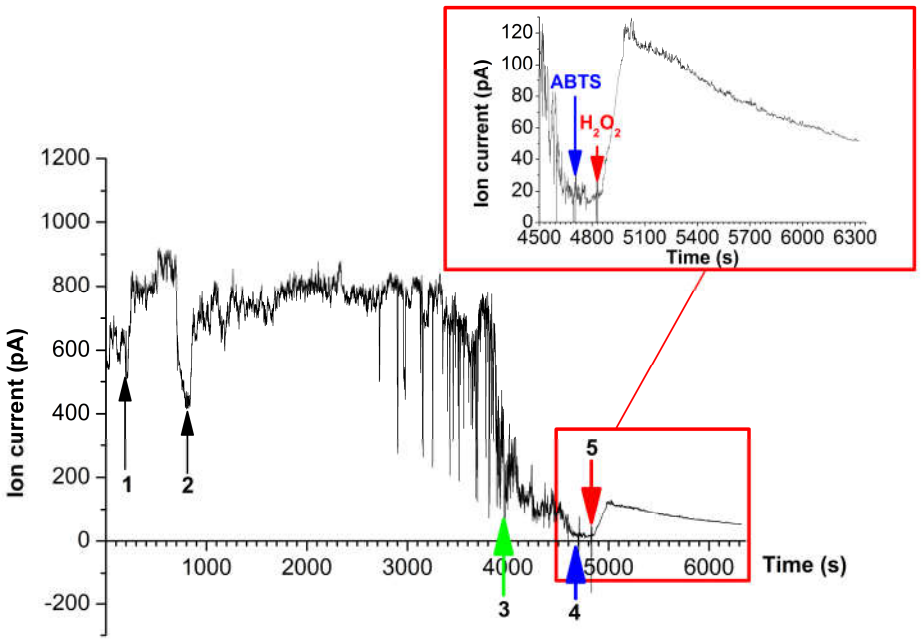

Figure 5. Typical time dependence of the ionic current recorded in the course of HRP-catalyzed oxidation of ABTS by hydrogen peroxide with an Axopatch 200B patch-clamp amplifier (operated at a bandwidth of 5 kHz) using a Si_3N_4 chip with a 16-nm-wide nanopore. Black arrows indicate time points of addition of the enzyme to

© 2026 by the author(s). Distributed under a Creative Commons CC BY license.

Preprints.org | NOT PEER-REVIEWED | Posted: 19 November 2026 https://doi.org/10.20944/preprints202611.1989.v1

the solution in the cis-chamber of the measuring cell (1, 2). Green arrow points at the moment of blockade of the nanopore by the enzyme (3). Blue (4) and red (5) arrows indicate time points of addition of ABTS (4) and H_2O_2 (5). Experimental conditions: 400 mV potential was applied to the cis-chamber; reaction medium was 0.1 M KCl solution (pH 5.5). The final concentrations of the HRP, ABTS and H_2O_2 in the cis-chamber were 1 μM, 0.3 mM and 2.5 mM, respectively. Inset shows the enlarged fragment of the *I(t)* curve marked with the red box.

The results obtained with narrow (9 nm) nanopores are in contrast to those obtained with wide (16 nm) ones: while the enzyme globules caused only shrinking of the wide nanopores and still passed through them, their adsorption on the walls of narrow pores caused more serious (though partial) blockade indicated by the green arrow in Figure 5. It should be emphasized that the shape of the *I(t)* curve changed markedly after the initiation of enzymatic reaction by the addition of H_2O_2 (red arrow in Figure 5). So far, the ionic current signal shown in the inset in Figure 5 can be ascribed to fluctuations of pore-confined enzyme globules in the course of enzymatic reaction. In our experiments reported, the nanopore-confined enzyme retained activity for 400 seconds.

3.4. Spectrophotometry

HRP is known to be enzymatically active against numerous organic and inorganic (such as potassium ferricyanide) [19] substrates. The optimum pH value, at which HRP exhibits highest enzymatic activity, differs considerably depending on buffer composition [20] and the substrate used [19]. Nevertheless, in fact, the enzyme remains functionally active over a broad pH range, including basic pH [20,21]. ABTS, guaiacol, o-phenylenediamine and 3,3′,5,5′-tetramethylbenzidine are quite frequently employed as chromogenic substrates in spectrophotometry-based techniques used for determination of HRP enzymatic activity [19,20,22]. One of the advantages of ABTS is the high (36 500 $M^{-1}cm^{-1}$ [19]) molar absorption coefficient of the respective cation-radical formed in the course of its HRP-catalyzed oxidation by hydrogen peroxide. Despite the ABTS substrate concentration is several orders of magnitude higher than the enzyme one [22–24], its value markedly influences the observed enzymatic activity of HRP [24].

In our experiments reported, we have tested the performance of HRP at various ABTS substrate concentrations in buffers with different values of pH and ionic strength in order to determine their usability in nanopore-based HRP activity studies. In parallel, experiments with performing CYP102A1-catalyzed monooxygenation of laurate in the presence of NADPH in the same media were performed in order to determine the usability of the solutions tested for different enzyme systems.

3.4.1. The Influence of Solution pH

Figure 6 displays typical $A_{405}(t)$ curves obtained at two different (0.03 mM and 0.15 mM) ABTS concentrations at an acidic pH of 4.0 and at a basic pH of 8.2.

© 2026 by the author(s). Distributed under a Creative Commons CC BY license.

Preprints.org | NOT PEER-REVIEWED | Posted: 19 November 2026 https://doi.org/10.20944/preprints202611.1989.v1

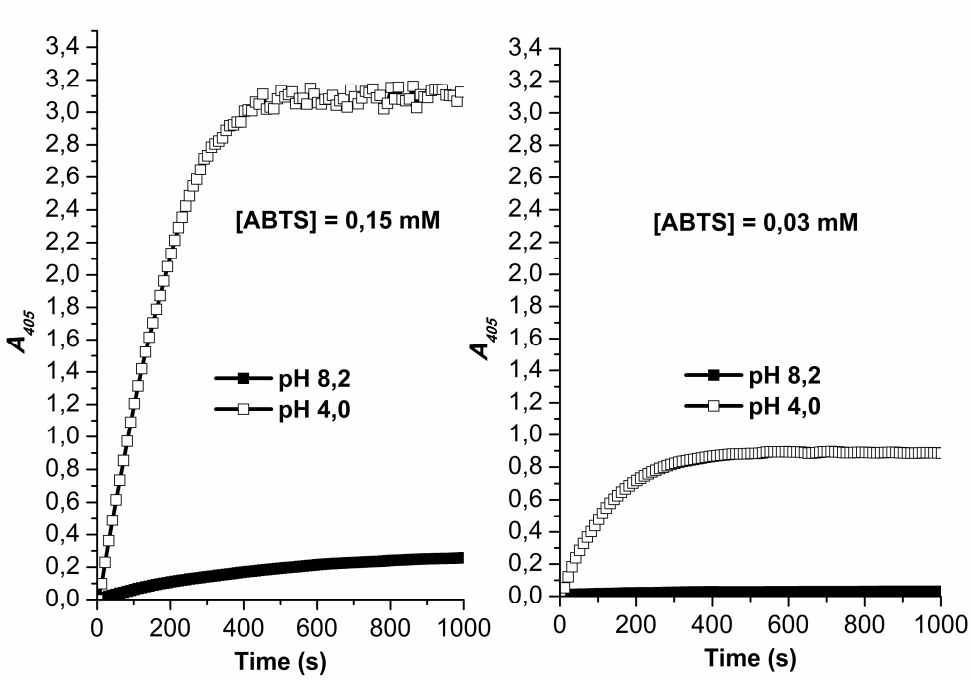

Figure 6. Typical time dependencies of absorbance recorded in the course of HRP-catalyzed oxidation of ABTS by hydrogen peroxide recorded with an Agilent 8453 spectrophotometer at 405 nm and a pathlength of 1 cm. Experimental conditions: reaction medium was either 1 mM potassium acetate buffer (pH 4.0; white squares) or 1 mM potassium borate buffer (pH 8.2; black squares). The final concentration of the enzyme in the cell was 1 nM; the concentration of ABTS was either 0.15 mM (left panel) or 0.03 mM (right panel), while the concentration of H_2O_2 was 2.5 mM in all cases.

As expected, the $A_{405}(t)$ curves shown in Figure 6 indicate much higher activity of HRP at acidic pH, and this result is in coincidence with previous studies [20,24,25]. Here, we should emphasize that higher (~0.3 mM) ABTS concentration is typically used in HRP enzymatic activity assays performed at acidic pH of 4.2 to 5.0 in the absence of chloride [22,23]. Nevertheless, it should be emphasized that an order of magnitude lower (0.036 to 0.04 mM) ABTS concentrations can also be employed even in neutral chloride-containing buffer (PBS [19]). Our results indicate that HRP retains activity against ABTS at a basic pH of 8.2 despite increased rate of suicide inactivation of the enzyme even at 2 mM H_2O_2 concentration at pH>8 [21]. With ABTS as substrate, the activity of HRP is detectable by spectrophotometry owing to the high molar extinction coefficient of ABTS cation-radical. In our experiments, we have reduced the concentration of ABTS in order to avoid its possible crystallization at high chloride concentrations. Namely, in our experiments, formation of crystals has been observed in borate buffer with a basic pH of 8.2 containing 0.6 M KCl at 0.3 mM ABTS concentration. Two-fold decrease of the ABTS concentration has allowed us to avoid its crystallization in the basic buffer with high chloride concentration. The ABTS concentration in acidic buffer has been reduced accordingly in order to compare the activity of the enzyme at two different pH values with keeping the ABTS concentration equal.

Figure 7 displays typical $A_{340}(t)$ curves obtained upon monitoring of CYP102A1 activity at an acidic pH of 4.0 and at a basic pH of 8.2.

© 2026 by the author(s). Distributed under a Creative Commons CC BY license.

Preprints.org | NOT PEER-REVIEWED | Posted: 19 November 2026 https://doi.org/10.20944/preprints202611.1989.v1

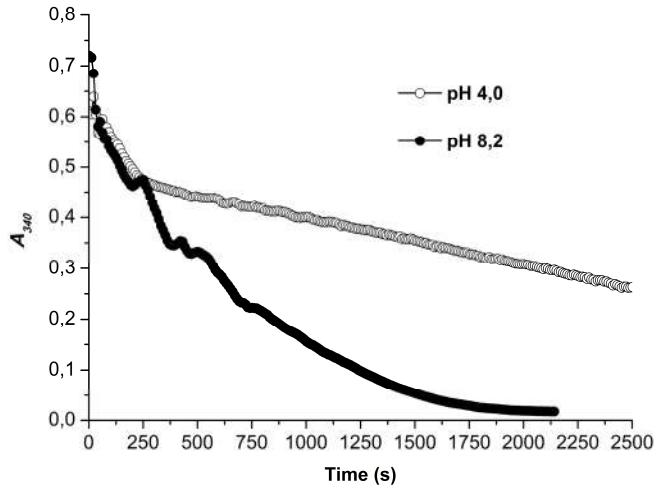

Figure 7. Typical time dependencies of absorbance recorded in the course of CYP102A1-catalyzed monooxygenation of laurate in the presence of NADPH recorded with an Agilent 8453 spectrophotometer at 340 nm and a pathlength of 1 cm. Experimental conditions: reaction medium was either 1 mM potassium acetate buffer (pH 4.0; white circles) or 1 mM potassium borate buffer (pH 8.2; black circles) containing 0.6 M KCl. The final concentration of the enzyme in the cell was 40 nM; the initial concentrations of laurate and NADPH were 500 μM and 200 μM, respectively.

The $A_{340}(t)$ curves shown in Figure 7 indicate that in the presence of 0.6 M KCl, the CYP102A1 enzyme is functional at both the acidic and the basic pH.

3.4.2. Enzymes' Performance at Neutral pH

With ABTS as substrate, HRP exhibits fastest performance at acidic pH [20], and this is employed in spectrophotometry-based techniques for determination of its enzymatic activity: the use of buffers with pH 4.2 [22] to 5.0 [23] is recommended. Nevertheless, at neutral pH of 7.0 to 7.4 HRP is still active in the reaction of ABTS oxidation [16,19]. Below, in Figure 8, we present the data on HRP performance in the reaction of ABTS oxidation at pH 7.4 and different buffer salts' concentrations.

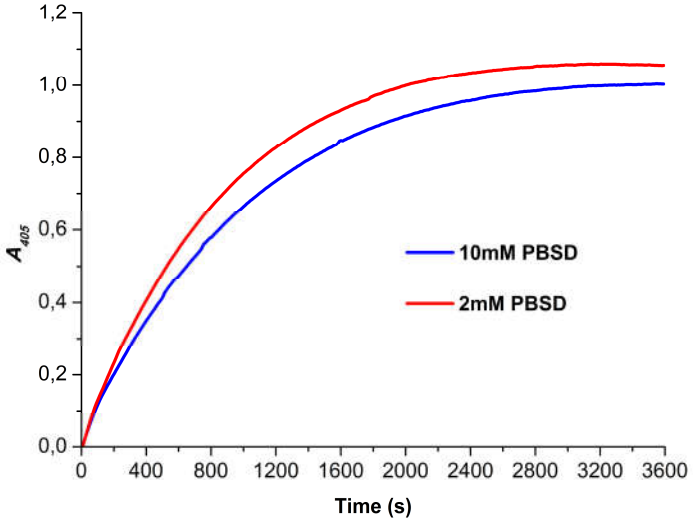

Figure 8. Typical time dependencies of absorbance recorded in the course of HRP-catalyzed oxidation of ABTS by hydrogen peroxide recorded with an Agilent 8453 spectrophotometer at 405 nm and a pathlength of 1 cm.

© 2026 by the author(s). Distributed under a Creative Commons CC BY license.

Preprints.org | NOT PEER-REVIEWED | Posted: 19 November 2026 https://doi.org/10.20944/preprints202611.1989.v1

Experimental conditions: reaction medium was either 2 mM (red) or 10 mM PBSD buffer (blue) with pH 7.2. The final concentration of the enzyme in the cell was 1 nM; the concentrations of ABTS and H_2O_2 were 0.3 mM and 2.5 mM, respectively.

The $A_{405}(t)$ curves shown in Figure 8 indicate that HRP enzymatic activity in 2 mM PBSD is comparable to that in 10 mM PBSD. The enzymatic performance of CYP102A1 has also been checked in 10 mM PBSD, and the respective data are shown in Figure 9.

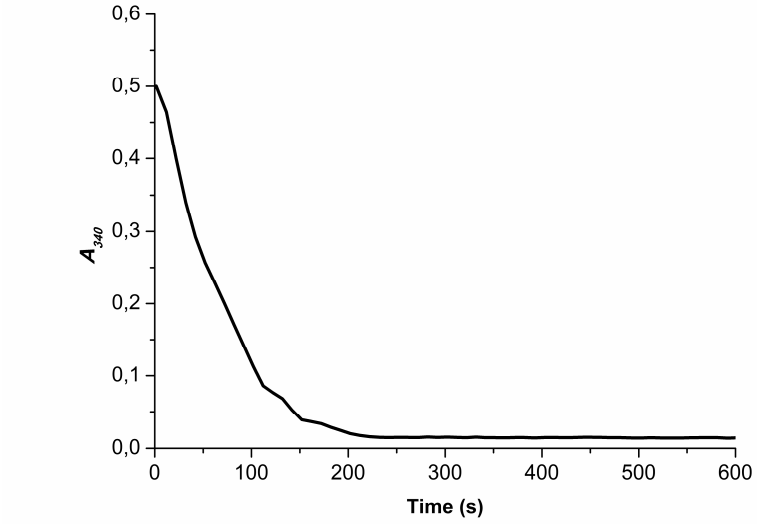

Figure 9. Typical time dependence of absorbance recorded in the course of CYP102A1-catalyzed monooxygenation of laurate in the presence of NADPH recorded with an Agilent 8453 spectrophotometer at 340 nm and a pathlength of 1 cm in 10 mM PBSD (pH 7.2). The final concentration of the enzyme in the cell was 40 nM; the initial concentrations of laurate and NADPH were 500 μM and 200 μM, respectively.

3.4.3. The Influence of Ionic Strength

Comparative spectrophotometric measurements were performed in deionized water without addition of buffer salts at various KCl concentrations. Figure 10 displays typical $A_{405}(t)$ curves obtained at various ionic strength obtained in this way.

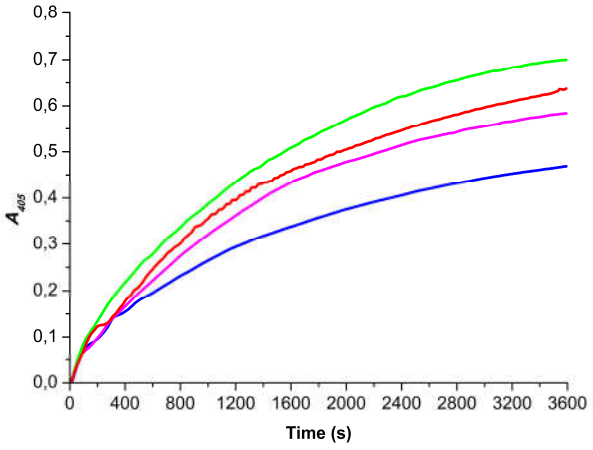

Figure 10. Typical time dependencies of absorbance recorded in the course of HRP-catalyzed oxidation of ABTS by hydrogen peroxide recorded with an Agilent 8453 spectrophotometer at 405 nm and a pathlength of 1 cm at

© 2026 by the author(s). Distributed under a Creative Commons CC BY license.

Preprints.org | NOT PEER-REVIEWED | Posted: 19 November 2026 https://doi.org/10.20944/preprints202611.1989.v1

various KCl concentrations. Experimental conditions: reaction medium was KCl solution with a concentration of 0 mM (pure water; blue), 0.06 M (magenta), 0.14 M (green) or 0.6 M (red). The final concentration of the enzyme in the cell was 1 nM; the concentrations of ABTS and H_2O_2 were 0.3 mM and 2.5 mM, respectively.

The data shown in Figure 10 indicate that in KCl solution (with an acidic pH of 5.5) HRP exhibits activity against ABTS over a broad range of KCl concentrations. In the presence of buffer salts, which stabilize pH at 7.2, the situation was different, as illustrated by the $A_{405}(t)$ curves shown in Figure 11.

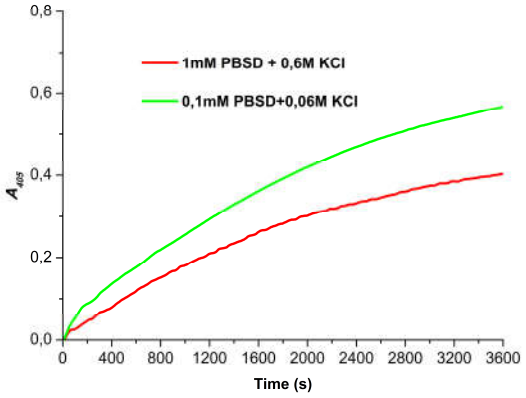

Figure 11. Typical time dependencies of absorbance recorded in the course of HRP-catalyzed oxidation of ABTS by hydrogen peroxide recorded with an Agilent 8453 spectrophotometer at 405 nm and a pathlength of 1 cm at various KCl concentrations in the presence of buffer salts, which stabilize the pH at 7.2 (PBSD). Experimental conditions: reaction medium was PBSD with added KCl: 0.1 mM PBSD and 0.06 M KCl (green) or 1 mM PBSD and 0.6 M KCl (red). The final concentration of the enzyme in the cell was 1 nM; the concentrations of ABTS and H_2O_2 were 0.3 mM and 2.5 mM, respectively.

It is interesting to note that at equal KCl concentration of 0.6 M, the final absorbance reached after one hour of observation in 1 mM PBSD was lower than that without pH-stabilizing buffer salts (Figure 11). This can be explained by lower (acidic) pH of KCl solution without added buffer salts [26]. Shu et al. reported the pH of 0.1 M KCl solution to be as low as 5.64 [26], what is close to the value of 5.5 obtained in our measurements.

The enzymatic activity of CYP102A1 has also been tested at various concentrations of KCl and in pure water (Figure 12).

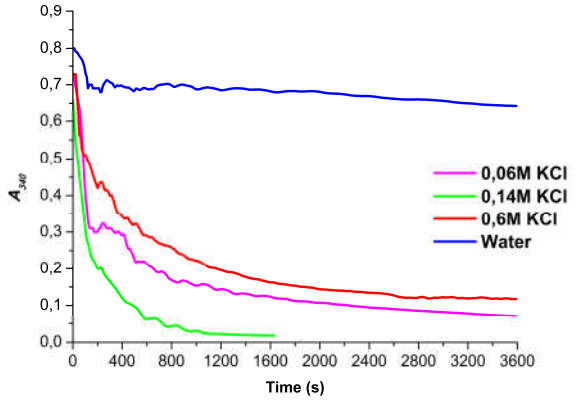

Figure 12. Typical time dependencies of absorbance recorded in the course of CYP102A1-catalyzed monooxygenation of laurate in the presence of NADPH recorded with an Agilent 8453 spectrophotometer at 340

© 2026 by the author(s). Distributed under a Creative Commons CC BY license.

Preprints.org | NOT PEER-REVIEWED | Posted: 19 November 2026 https://doi.org/10.20944/preprints202611.1989.v1

nm and a pathlength of 1 cm. Experimental conditions: reaction medium was KCl solution with a concentration of 0 mM (pure water; blue), 0.06 M (magenta), 0.14 M (green) or 0.6 M (red). The final concentration of the enzyme in the cell was 40 nM; the initial concentrations of laurate and NADPH were 500 μM and 200 μM, respectively.

The $A_{340}(t)$ curves shown in Figure 12 indicate that the presence of KCl even at 60 mM concentration promotes NADPH consumption. Similar situation was observed in the presence of pH-stabilizing buffer salts at phosphate concentration of 0.1 mM and 1 mM (Figure 13).

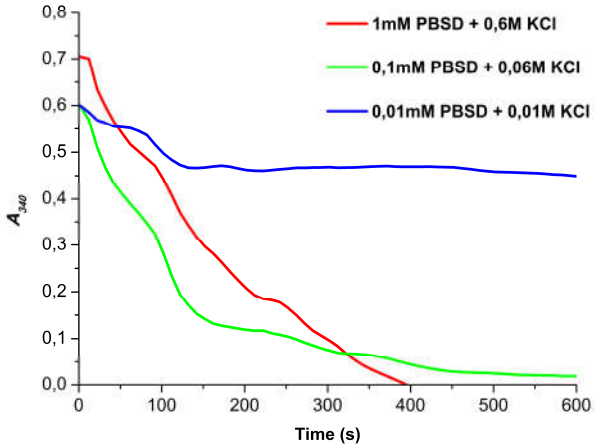

Figure 13. Typical time dependencies of absorbance recorded in the course of CYP102A1-catalyzed monooxygenation of laurate in the presence of NADPH recorded with an Agilent 8453 spectrophotometer at 340 nm and a pathlength of 1 cm. Experimental conditions: r reaction medium was PBSD with added KCl: 0.1 mM PBSD and 0.06 M KCl (green), 1 mM PBSD and 0.6 M KCl (red), or 0.01 mM PBSD and 0.01 M KCl (blue). The final concentration of the enzyme in the cell was 40 nM; the initial concentrations of laurate and NADPH were 500 μM and 200 μM, respectively.

The $A_{340}(t)$ curves shown in Figure 12 indicate that at very low (0.01 mM) concentrations of buffer salts and KCl the NADPH consumption occurs slowly — in contrast to the case with 0.1 mM PBSD with 0.06 M KCl added and 1 mM PBSD with 0.6 M KCl added.

4. Conclusions

The applicability of Si_3N_4 chips with 9 nm and 16 nm solid-state nanopores to the real-time monitoring of enzymatic activity of HRP in the reaction of ABTS oxidation by H_2O_2 has been tested. Translocation of single HRP globules through wider nanopores has been observed at 200 mV voltage applied to the cis-chamber of the solid state nanopore-based sensor device. This translocation has been observed despite adsorption of enzyme on the nanopore walls. The latter fact explains continued fluctuations of ionic current after switching the applied voltage to –200 mV. With narrower (9 nm) nanopores, the blockade of the nanopore lumen by the enzyme at an applied voltage of 400 mV was more serious, allowing the monitoring of enzymatic activity of pore-confined enzyme globules. The height of AFM images of HRP adsorbed on mica from 0.1 M KCl was 0.8 nm, indicating the existence of surface-adsorbed HRP in monomeric form under experimental conditions. The reference enzyme cytochrome P450 CYP102A1 (P450 BM3) adsorbed only on HOPG; at that, from 0.1 M KCl it adsorbed in the form of a mixture of monomeric and aggregated enzyme with heights of AFM images of up to 7 nm, while from 2 mM PBSD it adsorbed on HOPG predominantly as a monomer with heights of AFM images of 0.8 nm. By spectrophotometry, HRP enzymatic activity over a broad range of pH (from 4.0 to 8.2) has been confirmed. The functionality of HRP and CYP102A1 in both acidic

© 2026 by the author(s). Distributed under a Creative Commons CC BY license.

Preprints.org | NOT PEER-REVIEWED | Posted: 19 November 2026 https://doi.org/10.20944/preprints202611.1989.v1

potassium acetate buffer (pH 4.0) and basic potassium borate buffer (pH 8.2) with 0.6 M KCl added has been demonstrated.

Author Contributions: Conceptualization, Y.D.I.; methodology, Y.D.I. and I.D.S.; software, V.Y.T. and A.A.L.; validation, A.Y.D., O.F.P. and V.Y.T.; formal analysis, N.D.I. and O.N.A.; investigation, E.T.E., I.D.S., V.S.Z., A.N.A., A.F.K., A.A.S, E.E.V., and M.A.A.; resources, I.T.U., N.V.V., D.V.L., A.S.B. and I.S.M.; data curation, E.T.E., E.E.V., M.A.A., A.A.S., O.N.A. and I.T.U.; writing—original draft preparation, X.X.; writing—review and editing, Y.D.I. and I.D.S.; visualization, I.D.S.; supervision, Y.D.I.; project administration, Y.D.I.; funding acquisition, A.I.A. All authors have read and agreed to the published version of the manuscript.

Funding: Atomic force microscopy, spectrophotometry and measurements with the solid-state nanopore-based detector were performed within the framework of the Program for Basic Research in the Russian Federation for a long-term period (2021-2030) (No. 122030100168-2). The experimental work on the surface modification of AFM and nanopore chips was supported by the Ministry of Science and Higher Education of the Russian Federation (State Assignment No. 075-00270-26-00).

Data Availability Statement: The data underlying the results reported can be obtained from the corresponding author upon reasonable request.

Conflicts of Interest: The authors declare no conflict of interest.

References

1. Xie, X.S.; Lu, H.P. Single-molecule Enzymology. *J. Biol. Chem*. **1999**, *274*, 15967–15970. https://doi.org/10.1074/jbc.274.23.15967.
2. Shumov, I.D.; Ziborov, V.S.; Ableev, A.N.; Vinogradova, A.V.; Afonin, O.N.; Bukharina, N.S.; Vaulin, N.V.; Lebedev, D.V.; Bukatin, A.S.; Mukhin, I.S.; Saraeva, I.N.; Archakov, A.I.; Ivanov, Y.D. Nanotechnology-based sensors for monitoring single molecules of cytochrome P450 BM3. *Appl. Phys. (Russian).* **2026,** *2,* 79–84. https://doi.org/10.51368/2949-561X-2026-2-79-84.
3. Vazhenkova, E.E.; Shumov, I.D.; Zhdanov, D.D.; Shumyantseva, V.V.; Ziborov, V.S.; Ableev, A.N.; Afonin, O.N.; Vaulin, N.V.; Lebedev, D.V.; Bukatin, A.S.; Mukhin, I.S.; Tatur, V.Y.; Lukyanitsa, A.A.; Ponomarenko, E.A.; Archakov, A.I.; Ivanov, Y.D. Study of changes in the adsorption properties of L-asparaginase on mica under thermal action for the development of a nanopore-based detector. *Appl. Phys. (Russian).* **2026,** *3,* 89–94. https://doi.org/10.51368/2949-561X-2026-3-93-98.
4. Ivanov, Y.D.; Bukharina, N.S.; Shumov, I.D.; Afonin, O.N.; Tatur, V.Y.; Grudo, A.V.; Archakov, A.I. AFM-Based Monitoring of Enzymatic Activity of Individual Molecules of Cytochrome CYP102A1. *Biosensors* **2025**, *15*, 303. https://doi.org/10.3390/bios15050303
5. Radmacher, M.; Fritz, M.; Hansma, H.G.; Hansma, P.K. Direct Observation of Enzyme Activity with the Atomic Force Microscope. *Science* **1994**, *265*, 1577–1579. https://doi.org/10.1126/science.8079171.
6. Pham, B.; Eron, S.J.; Hill, M.E.; Li, X.; Fahie, M.A.; Hardy, J.A.; Chen, M. A nanopore approach for analysis of caspase-7 activity in cell lysates. *Biophys. J*. **2019**, *117*, 844–855. https://doi.org/10.1016/j.bpj.2019.07.045.
7. Wang, L.; Han, Y.; Zhou, S.; Guan, X. Real-time label-free measurement of HIV-1 protease activity by nanopore analysis. *Biosens. Bioelectron*. **2014**, *62*, 158–162. https://doi.org/10.1016/j.bios.2014.06.041.
8. Zhou, S.; Wang, L.; Chen, X.; Guan, X. Label-free nanopore single-molecule measurement of trypsin activity. *ACS Sensors* **2016**, *1 (5)*, 607–613. https://doi.org/10.1021/acssensors.6b00043.
9. Kukwikila, M.; Howorka, S. Nanopore-based electrical and label-free sensing of enzyme activity in blood serum. *Anal. Chem*. **2015**, *87 (18)*, 9149–9154. https://doi.org/10.1021/acs.analchem.5b01764.
10. Ivanov, Y.D.; Ableev, A.N.; Shumov, I.D.; Ivanova, I.A.; Vaulin, N.V.; Lebedev, D.V.; Bukatin, A.S.; Mukhin, I.S.; Archakov, A.I. Registration of Functioning of a Single Horseradish Peroxidase Macromolecule with a Solid-State Nanopore. *Int. J. Mol. Sci.* **2023**, *24*, 15636. https://doi.org/10.3390/ijms242115636.

© 2026 by the author(s). Distributed under a Creative Commons CC BY license.

Preprints.org | NOT PEER-REVIEWED | Posted: 19 November 2026 https://doi.org/10.20944/preprints202611.1989.v1

11. Ivanov, Y.D.; Vinogradova, A.V.; Nevedrova, E.D.; Ableev, A.N.; Kozlov, A.F.; Shumov, I.D.; Ziborov, V.S.; Afonin, O.N.; Vaulin, N.V.; Lebedev, D.V.; et al. Solid-State Nanopore-Based Nanosystem for Registration of Enzymatic Activity of a Single Molecule of Cytochrome P450 BM3. *Int. J. Mol. Sci.* **2024**, *25*, 10864. https://doi.org/10.3390/ijms251910864
12. Dekker, C. Solid-state nanopores. *Nat. Nanotechnol.* **2007**, *2*, 209–215. https://doi.org/10.1038/nnano.2007.27.
13. Tan, S.W.; Gu, D.J.; Liu, H.; Liu, Q.J. Detection of a single enzyme molecule based on a solid-state nanopore sensor. *Nanotechnology* **2016**, *27*, 155502. https://doi.org/10.1088/0957-4484/27/15/155502.
14. Yao, Y.; Zhang, B.; Pang, H.; Wang, Y.; Fu, H.; Chen, X.; Wang, Y. The effect of radio frequency heating on the inactivation and structure of horseradish peroxidase. *Food Chem*. **2023**, *398*, 133875. https://doi.org/10.1016/j.foodchem.2022.133875.
15. Krainer, F.W.; Glieder, A. An updated view on horseradish peroxidases: recombinant production and biotechnological applications. *Appl Microbiol Biotechnol*. **2015,** *99*, 1611–1625. https://doi.org/10.1007/s00253-014-6346-7.
16. Ivanov, Y.D.; Ableev, A.N.; Vinogradova, A.V.; Nevedrova, E.D.; Shumov, I.D.; Ziborov, V.S.; Kozlov, A.F.; Ivanova, I.A.; Vaulin, N.V.; Lebedev, D.V.; Bukatin, A.S.; Mukhin, I.S.; Ponomarenko, E.A.; Archakov, A.I. Registration of activity of a single molecule of horseradish peroxidase using a detector based on a solid-state nanopore. *Biomeditsinskaya Khimiya* **2024**, *70 (5)*, 349–355. https://doi.org/10.18097/PBMC20247005349.
17. Kiselyova, O.I.; Yaminsky, I.; Ivanov, Y.D.; Kanaeva, I.P.; Kuznetsov, V.Y.; Archakov, A.I. AFM study of membrane proteins, cytochrome P450 2B4, and NADPH–Cytochrome P450 reductase and their complex formation. *Arch. Biochem. Biophys.* **1999**, *371*, 1–7. https://doi.org/10.1006/abbi.1999.1412.
18. Ivanov, Y.D.; Pleshakova, T.O.; Shumov, I.D.; Kozlov, A.F.; Ivanova, I.A.; Valueva, A.A.; Tatur, V.Y.; Smelov, M.V.; Ivanova, N.D.; Ziborov, V.S. AFM imaging of protein aggregation in studying the impact of knotted electromagnetic field on a peroxidase. *Sci. Rep.* **2020**, *10*, 9022. https://doi.org/10.1038/s41598-020-65888-z.
19. Zhang, H.; Gao, G.; Fan, Y.; Zhi, J. Revisiting the catalytic activity of single horseradish peroxidase clusters through electrochemical collision technique: Effect of electrolyte and substrate. *Talanta* **2025,** *282,* 126951. https://doi.org/10.1016/j.talanta.2024.126951.
20. Drozd, M.; Pietrzak, M.; Parzuchowski, P.G.; Malinowska, E. Pitfalls and capabilities of various hydrogen donors in evaluation of peroxidase-like activity of gold nanoparticles. *Anal. Bioanal. Chem.* **2016**, *408*, 8505–8513. https://doi.org/10.1007/s00216-016-9976-z.
21. Malomo, S.O.; Adeoye, R.I.; Babatunde, L.; Saheed, I.A.; Iniaghe, M.O.; Olorunniji, F.J. Suicide inactivation of horseradish peroxidase by excess hydrogen peroxide: The effects of reaction pH, buffer ion concentration, and redox mediation. *Biokemistri* **2011,** *23 (3),* 124 – 128.
22. Porstmann, B.; Porstmann, T.; Nugel, E. Comparison of Chromogens for the Determination of Horseradish Peroxidase as a Marker in Enzyme Immunoassay. *J. Clin. Chem. Clin. Biochem*. **1981,** *19,* 435–439. https://doi.org/10.1515/cclm.1981.19.7.435.
23. Sanders, S.A.; Bray, R.C.; Smith, A.T. pH-dependent properties of a mutant horseradish peroxidase isoenzyme C in which Arg38 has been replaced with lysine. *Eur. J. Biochem.* **1994**, *224*, 1029–1037. https://doi.org/10.1111/j.1432-1033.1994.01029.x.
24. Gallati, H. Peroxidase aus Meerrettich: Kinetische Studien sowie Optimierung der Aktivitätsbestimmung mit den Substraten H_2O_2 und 2,2'-Azino-di-(3-ethyl-benzthiazolinsulfonsäure-(6)) (ABTS). *J. Clin. Chem. Clin. Biochem*. **1979,** *17,* 1–7. https://doi.org/10.1515/cclm.1979.17.1.1.
25. Wasak, A.; Drozd, R.; Jankowiak, D.; Rakoczy, R. The influence of rotating magnetic field on bio-catalytic dye degradation using the horseradish peroxidase. *Biochem. Eng. J.* **2019**, *147*, 81–88, https://doi.org/10.1016/j.bej.2019.04.007.
26. Shu, L.; Lu, X.; Jegatheesan, V.; Jegatheesan, L. Investigating pH and other electrical properties of potassium salt solutions. *Food Chem. Adv.* **2023**, *2*, 100210. https://doi.org/10.1016/j.focha.2023.100210.

Disclaimer/Publisher's Note: The statements, opinions and data contained in all publications are solely those of the individual author(s) and contributor(s) and not of MDPI and/or the editor(s). MDPI and/or the editor(s) disclaim responsibility for any injury to people or property resulting from any ideas, methods, instructions or products referred to in the content.

© 2026 by the author(s). Distributed under a Creative Commons CC BY license.